Geoscience Frontiers xxx (xxxx) xxx

Contents lists available at ScienceDirect

Geoscience Frontiers

journal homepage: www.elsevier.com/locate/gsf

Research Paper

Assessment of SARS-COV-2 airborne infection transmission risk in public buses

M. Bertone [a], A. Mikszewski [b,c], L. Stabile [a,*], G. Riccio [d], G. Cortellessa [a], F.R. d'Ambrosio [e], V. Papa [f], L. Morawska [c], G. Buonanno [a,c]

[a] Department of Civil and Mechanical Engineering, University of Cassino and Southern Lazio, Cassino, FR, Italy
[b] CIUS Building Performance Lab, The City University of New York, New York, NY, USA
[c] International Laboratory for Air Quality and Health, Queensland University of Technology, Brisbane, Queensland, Australia
[d] Department of Industrial Engineering, University of Naples "Federico II", Italy
[e] Department of Industrial Engineering, University of Salerno, Italy
[f] Department of Motor Sciences and Wellness, University of Naples "Parthenope", Italy

ARTICLE INFO

Article history:
Received 12 October 2021
Revised 25 March 2022
Accepted 11 April 2022
Available online xxxx

Keywords:
SARS-CoV-2
Airborne transmission
Bus
Transport microenvironment
Maximum occupancy
Air exchange rate

ABSTRACT

Public transport environments are thought to play a key role in the spread of SARS-CoV-2 worldwide. Indeed, high crowding indexes (i.e. high numbers of people relative to the vehicle size), inadequate clean air supply, and frequent extended exposure durations make transport environments potential hotspots for transmission of respiratory infections. During the COVID-19 pandemic, generic mitigation measures (e.g. physical distancing) have been applied without also considering the airborne transmission route. This is due to the lack of quantified data about airborne contagion risk in transport environments.

In this study, we apply a novel combination of close proximity and room-scale risk assessment approaches for people sharing public transport environments to predict their contagion risk due to SARS-CoV-2 respiratory infection. In particular, the individual infection risk of susceptible subjects and the transmissibility of SARS-CoV-2 (expressed through the reproduction number) are evaluated for two types of buses, differing in terms of exposure time and crowding index: urban and long-distance buses. Infection risk and reproduction number are calculated for different scenarios as a function of the ventilation rates (both measured and estimated according to standards), crowding indexes, and travel times. The results show that for urban buses, the close proximity contribution significantly affects the maximum occupancy to maintain a reproductive number of <1. In particular, full occupancy of the bus would be permitted only for an infected subject breathing, whereas for an infected subject speaking, masking would be required. For long-distance buses, full occupancy of the bus can be maintained only if specific mitigation solutions are simultaneously applied. For example, for an infected person speaking for 1 h, appropriate filtration of the recirculated air and simultaneous use of FFP2 masks would permit full occupancy of the bus for a period of almost 8 h. Otherwise, a high percentage of immunized persons (>80%) would be needed.

1. Introduction

The COVID-19 pandemic, caused by the SARS-CoV-2 virus, has disrupted modern society and presented a significant challenge to indoor environments, where virus transmission mainly occurs (Blocken et al., 2020; Luo et al., 2020; Chang et al., 2021; Miller et al., 2021; Morawska et al., 2021). Among the different pathways of infection transmission, the World Health Organization (WHO) and the US Centers for Disease Control and Prevention (CDC) (WHO, 30 April 2021; US CDC, 7 May 2021) have eventually recognized the airborne transmission of inhalable airborne respiratory particles (i.e. particles below 100 μm in diameter capable of remaining suspended in the air) as the dominant mode of respiratory infection in indoor environments with respect to spray borne particles (larger particles quickly settling due to their inertia), and fomites (i.e. contaminated surfaces) (Morawska and Milton, 2020; Kriegel et al., 2020; Marr and Tang, 2021; Miller et al., 2021). Thus, indoor environments with a high crowding index (number of people relative to the room size) and inadequate clean (pathogen-free)

* Corresponding author.
E-mail address: l.stabile@unicas.it (L. Stabile).

https://doi.org/10.1016/j.gsf.2022.101398

air supply represent sites where the highest risk of microbial infection occurs (Li et al., 2007; Buonanno et al., 2020a; Correia et al., 2020; Miller et al., 2021). During the COVID-19 pandemic, the measures implemented by governments have not been targeted to reduce the transmission of the virus for all three mechanisms of transmission (airborne respiratory particles, sprayborne respiratory particles, and fomites). Indeed, the primary mitigation measures adopted have been physical distancing and hand hygiene, which address sprayborne respiratory particles and contaminated surfaces, but have limited effectiveness on transmission through airborne respiratory particles (Chen et al., 2020). This is due to the lack of data relating to quantified airborne contagion risk in indoor environments. Indeed, the first experimental evidence of SARS-CoV-2 RNA concentration in indoor air in the presence of an infected person (Lednicky et al., 2020; Liu et al., 2020; Nissen et al., 2020; Stern et al., 2021) as well as traces of SARS-CoV-2 RNA on air conditioning filters and ambient air in buses (Moreno et al., 2021) were only recently reported in the scientific literature. Thus, given the millions of commuters using public transport every day in the world, there is an obvious need for further information on the risk of airborne contagion so that effective prevention measures can be implemented. In particular, airborne transmission of SARS-CoV-2 on buses has emerged as a concern in light of multiple outbreaks since the onset of the pandemic (Luo et al., 2020; Shen et al., 2020). Buses have historically been associated with transmission of *Mycobacterium tuberculosis* (Mohr et al., 2012) and measles virus (Perkins et al. 1947; Helfand et al., 1998), with one case report for variola (smallpox) virus (Suleimanov and Mandokhel, 1972). Therefore, mitigation of airborne transmission of respiratory pathogens on buses represents an important topic even beyond the COVID-19 pandemic.

The significance of airborne transmission has highlighted the need to have appropriate pathogen-free air supply rates (i.e. air exchange rates) to reduce the spread of SARS-CoV-2 (Buonanno et al., 2020a; Morawska et al., 2021; Stabile et al., 2021). Despite numerous studies quantifying air exchange rates in indoor microenvironments, no existing ventilation standard so far developed by national authorities or international professional societies (e.g. ASHRAE 62.1 [2019]) takes into consideration the requirements for infection control in non-healthcare settings (Morawska et al., 2021). In addition, there are no specific technical regulations or standards for buses focused on ventilation and air exchange rate. Regulation n°107 of the UNECE (United Nations Economic Commission for Europe) on the uniform provisions concerning the approval of vehicles, including buses, does not consider the ventilation systems and defines the maximum bus capacity considering only the available internal surface and the maximum permissible load. Nevertheless, some countries have a standard for buses; for example, the German standard VDV 236 (2015) requires 15 $m^3\ h^{-1}$-person^{-1} of clean air, and the Chinese standard JT/T 888 (2014) requires 20 $m^3\ h^{-1}$ person^{-1} of clean air.

The purpose of this study was to quantify the risk of airborne transmission in buses and identify mitigation strategies to reduce the transmission potential of SARS-CoV-2 infection for safe transportation of passengers and to control the spread of the pandemic. To this end, we performed risk assessment simulations considering airborne transmission both in close proximity to an infected passenger (i.e. within 1.5 m) and at more distant locations in the bus breathing shared air (referred to as "room-scale"). For the close proximity component, we applied a computational fluid dynamics (CFD) approach, whereas for the room-scale component we applied a simplified zero-dimensional model based on a virus mass balance that allows prospective analyses. Simulations were performed considering various exposure scenarios in the bus environment taking into account the characteristics of the emitting subject, microenvironment, ventilation, and exposed subjects also including the effect of mitigation strategies. As the Delta variant (B.1.617.2 SARS-CoV-2) is now dominant across much of the world, and is recognized as more infectious than previous variants, the risk assessment proposed here focuses on this variant.

2. Materials and methods

To quantify the risk of airborne transmission of viruses in buses and to identify mitigation strategies to reduce the transmission potential of SARS-CoV-2 infection for safe transportation of commuters, the approaches proposed by Cortellessa et al. (2021) and Buonanno et al. (2020a) are used. In particular, we evaluate airborne transmission resulting from inhaling virus-laden airborne particles at two different spatial scales: i) in *close proximity*, i.e. within approximately 1.5 m of an emitting subject; and ii) at *room-scale*, i.e. sharing the same indoor environment of the infected subject and then inhaling particles that remain suspended in air. The dichotomy of close proximity versus room-scale airborne transmission has also been referred to as short-range versus long-range transmission (Chen et al., 2020). Individual risk of infection (i.e. the ratio between the number of new infections and the number of exposed susceptible individuals, hereinafter referred as IR_{cp} and IR_{rs}) and reproductive number (i.e. the expected number of new infections arising from a single infectious individual, hereinafter referred as R_{cp} and R_{rs}) for both close proximity and room-scale are evaluated adopting an exposure-to-risk approach developed and presented in our previous papers (Buonanno et al., 2020a,b; Stabile et al., 2021). This approach is summarized and customized for close proximity and room-scale assessments. Different scenarios are studied with ventilation rates estimated according to regulatory standards and measured through an *ad-hoc* experimental campaign and crowding indexes required by regulatory authorities.

2.1. Evaluation of the individual risk of infection and reproductive number for close proximity transmission

The close proximity approach consists of a Eulerian-Lagrangian based model for the analysis of respiratory particle dispersion in close proximity represented by a breathing/speaking infected subject (emitter) and a susceptible subject (receiver) in the case of face-to-face orientation and stagnant air conditions. A CFD technique is adopted for the three-dimensional numerical description of velocity, pressure, and temperature fields, along with the motion and interaction of the respiratory particles with the fluid. The fully opensource finite volume based OpenFOAM software is employed as a fully open and flexible tool with complete control of the variables chosen for particle dispersion assessment. The adopted Lagrangian particle tracking (LPT) approach is based on a dispersed dilute two-phase flow and allows the respiratory particle motion inside the air flow to be determined. In particular, the spacing between respiratory particles in the exhaled air plume is sufficiently large and the volume fraction of the respiratory particles is sufficiently low ($<10^{-3}$) to justify the use of a Eulerian-Lagrangian approach, in which the continuum equations are solved for the air flow (continuous phase) and Newton's equation of motion is solved for each respiratory particle. The continuity equations are widely described in the available scientific literature (Massarotti et al., 2006; Scungio et al., 2013; Arpino et al., 2014) while the respiratory particle motion equations, solved for an unsteady incompressible Newtonian fluid and considering the drag and gravity forces acting on the particle, are described in Cortellessa et al. (2021) and not reported here for brevity. Further details are reported in the Supplementary Material where the particle emission rates as a function of the particle size for breathing

activity are also summarized (Table S1). Particle emission rates adopted for close proximity modeling were obtained considering peak flow rates and velocities at the mouth of the infected subject in order to simulate the worst condition (i.e. adopting a conservative approach) in terms of risk of infection due to the close proximity route of transmission.

The close proximity airborne transmission risk is evaluated using the volumetric dose of airborne particles pre-evaporation ($V_{\text{d-airborne-pre}}$) inhaled by a susceptible person during face-to-face interaction with an infected person in one minute of exposure (mL min^{-1}). We use the pre-evaporation volume because the dose of RNA copies inhaled relates to the original volume rather than the evaporated volume, as particles retain their RNA load while losing water during the instantaneous evaporation occurring upon expiration. This dose of inhaled RNA copies can be approximated as the product of $V_{\text{d-airborne-pre}}$ (mL min^{-1}), the viral load (c_v, RNA copies mL^{-1}) of the infected person, and the duration of face-to-face interaction (T, min). Values for $V_{\text{d-airborne-pre}}$ when the infected person is speaking are taken from Cortellessa et al. (2021) for separation distances of up to 1.75 m, whereas original estimates for $V_{\text{d-airborne-pre}}$ when the infected person is breathing only for separation distances of up to 0.5 m are reported in the Supplementary Material (Table S2). CFD models for both speaking and breathing activities do not consider mask use because masks completely alter the close proximity particle flow regime, thus reducing the close proximity risk. In our calculation we consider that the close proximity risk is negligible in a scenario where the infected person wears a mask.

To model c_v, we used the preliminary data posted by von Wintersdorff et al. (2021) that confirms that higher c_v values are associated with Delta variant infections; in particular, we fit the statistical distribution of the c_v data obtained by von Wintersdorff et al. (2021) on their 87 sequence-confirmed Delta variant infection data with a lognormal c_v distribution, yielding a mean and standard deviation of 7.1 and 0.70 $\log_{10}$ RNA copies mL^{-1}, respectively.

To calculate the probability of infection (P_I, %) from close proximity airborne transmission, we used a common exponential dose–response model as follows:

$$P_I = 1 - e^{-\frac{c_v \cdot V_{\text{d-airborne-pre}} \cdot T}{\text{HID}_{63}}}(\%) \quad (1)$$

where HID_{63} represents the human infectious dose for 63% of susceptible subjects. For the Delta variant, a HID_{63} value of 700 RNA copies was adopted based on the thermodynamic equilibrium dose–response model of Gale (2020). We point out that the term ($c_v \cdot V_{\text{d-airborne-pre}} \cdot \text{T}/\text{HID}_{63}$) represents the term hereafter referred to as "dose of quanta" (D_q).

The close proximity individual risk of infection (IR_{cp}) of the exposed person was then calculated by integrating, for all the possible c_v values, the product between the conditional probability of the infection for each c_v ($P_I(c_v)$) and the probability of occurrence of each c_v value (P_{cv}):

$$IR_{cp} = \int_{c_v} (P_I(c_v) \bullet P_{cv}) \text{d}c_v(\%) \quad (2)$$

For the purposes of our modelling analysis, we assume an infected person on a bus has close proximity interaction (speaking or breathing) with only one susceptible person; in other words, just one susceptible person is within 1.5 m and in a face-to-face orientation for the whole exposure time (i.e. travel time). This hypothesis of perfect face-to-face orientation amongst infected and susceptible persons is the most critical scenarios; indeed, this condition maximizes the risk of infection of the exposed subject. As a result, the close proximity reproduction number (R_{cp}) (i.e. the number of secondary cases amongst the susceptibles in close proximity to an infected subject) is equivalent to the close proximity individual risk of infection (IR_{cp}).

2.2. Evaluation of the individual risk of infection and reproductive number for room-scale transmission

The room-scale approach is based on a box model in which a virus mass balance equation is applied, estimating the emission of an infected subject and predicting exposure concentrations and infection risks for prospective scenarios. The approach is based on the following hypotheses: the emitted particles are instantaneously and evenly distributed in the environment, and the latent period of the disease is longer than the time of the model (Gammaitoni and Nucci, 1997). Infected people breathing and/or speaking and susceptible people sitting and/or standing (in case of urban buses) are considered.

For room-scale airborne transmission assessment, the predictive estimation approach developed by Buonanno et al. (2020a, b), and already applied in Moreno et al. (2021) and Stabile et al. (2021), was adopted. The approach requires six steps: (i) evaluation of the quanta emission rate (hereinafter referred as ER_q, quanta h^{-1}); (ii) estimation of the exposure to quanta concentration in the environment (referred as $n(t,ER_q)$); (iii) evaluation of the dose of quanta received by exposed subjects ($D_q(ER_q)$); (iv) estimation of the probability of infection based on a dose–response model ($P_I(ER_q)$); (v) evaluation of the individual risk of the exposed person (IR_{rs}); and (vi) evaluation of the room-scale reproduction number (R_{rs}) based on crowding. The abovementioned quantum is defined as an inhaled dose of RNA copies of SARS-CoV-2 that can cause infection in 63% of susceptible people in an indoor environment, whereas the quanta emission rate is the number of quanta released into the air per unit of time as a function of the expiratory activities of an infected subject, respiratory parameters, and activity levels. The approach estimates the quanta emission rate of an infectious subject based on the viral load in the respiratory fluid and the concentration of particles expired during different activities; moreover, it considers the metabolic rate and respiratory activity of the emitting subject and the activity of the exposed subject.

This approach represents an important step forward, as previously the viral load emitted was difficult to estimate; in fact, a backward calculation was used to estimate the emission of an infected subject based on retrospective assessments of outbreaks only at the end of an epidemic (Myatt et al., 2008; Rudnick and Milton, 2003; Sze To and Chao, 2010; Wagner, Coburn and Blower, 2009).

The quanta emission rate (ER_q, quanta h^{-1}) is evaluated as:

$$ER_q = c_v \cdot c_i \cdot IR \cdot V_d(\text{quanta h}^{-1}) \quad (3)$$

where c_v (RNA copies mL^{-1}) is the viral load in the saliva (as defined in Section 2.1), c_i (quanta RNA copies) is a conversion factor defined as the ratio between one infectious quantum and the infectious dose expressed in viral RNA copies (assumed as in Section 2.1), IR is the inhalation rate (m^3 h^{-1}) of the infected subject, which is a function of the subject's activity level and age, and V_d is the droplet volume concentration expelled by the infectious person (mL m^{-3}). IR and V_d data are reported in Buonanno et al. (2020a). The resulting statistical distributions of the quanta emission rate values (ER_q, quanta h^{-1}), expressed as $\log_{10}$ (average ± standard deviation), are 1.19 ± 0.68 and 1.84 ± 0.68 for oral breathing and speaking, respectively.

The indoor quanta concentration in the environment $n(t,ER_q)$ is evaluated for each possible ER_q value using the equation:

$$n(t, ER_q) = n_0 \cdot e^{-IVRR \cdot t} + \frac{ER_q \cdot I}{IVRR \cdot V} \cdot (1 - e^{-IVRR \cdot t})(\text{quanta m}^{-3}) \quad (4)$$

where n_0 (quanta m^{-3}) is the initial quanta concentration in the bus (assumed to be zero), $IVRR$ (h^{-1}) represents the infectious virus removal rate and is the sum of three contributions (Yang and Marr, 2011): (i) AER (h^{-1}), the air exchange rate; (ii) k (h^{-1}), the particle deposition rate on surfaces (equal to 0.24 h^{-1}, (Chatoutsidou and Lazaridis, 2019)); (iii) λ (h^{-1}), the viral inactivation rate (equal to 0.63 h^{-1}, (van Doremalen et al., 2020)); I is the number of infectious subjects, and V is the volume of the buses considered.

The dose of quanta received by an exposed subject (D_q) to a certain quanta concentration, $n(t,ERq)$, for a certain exposure time, t, can be evaluated by integrating the quanta concentration over time as:

$$D_q(ER_q) = IR \cdot \int_0^t n(t)\mathrm{d}t(\text{quanta}) \quad (5)$$

Here IR represents the inhalation rate of the exposed subjects that, once again, depends on their activity level and age.

The probability of infection (PI, %) of exposed persons is evaluated based on the same exponential dose–response model considered for close proximity:

$$P_I(ER_q) = 1 - e^{-D_q(ER_q)}(\%) \quad (6)$$

Once again, we point out that close proximity and room-scale approaches are based on the same exposure-to-risk evaluation; indeed, Eq. (6) is practically the same as Eq. (1).

The room-scale individual infection risk of an exposed person (IR_{rs}) is calculated by integrating, for all the possible ER_q values, the product between the conditional probability of the infection for each ER_q ($P_I(ER_q)$) and the probability of occurrence of each ER_q value (P_{ERq}):

$$IR_{rs} = \int_{ER_q} (P_I(ER_q) \cdot P_{ER_q})\mathrm{d}ER_q(\%) \quad (7)$$

The room-scale reproduction number (R_{rs}) represents the expected number of secondary cases arising from the exposure and is simply calculated as the product of IR_{rs} and the number of susceptible passengers on the bus. When considering both close proximity and room-scale airborne transmission, the total number of expected secondary cases arising from the bus trip (R_{event}) is the sum of R_{cp} and R_{rs}.

With a view towards minimizing the spread of infection, such that the bus exposure results in fewer than one secondary transmission on average, the number of susceptible passengers should be monitored to maintain a condition where $R_{event} < 1$. To this end, the maximum number of susceptibles that can stay simultaneously in the confined space under investigation for an acceptable $R_{event} < 1$ (hereafter referred to as maximum room occupancy, MRO), considering a single close proximity interaction and room-scale airborne transmission, is:

$$MRO = \frac{1 - IR_{cp}}{IR_{rs}}(\text{susceptibles}) \quad (8)$$

2.3. Scenarios

The individual infection risk of susceptible subjects and the overall transmission potential (expressed as reproduction number) are evaluated for two types of buses, differing in terms of exposure time and crowding index, as follows: i) urban buses (class I) characterized by a short exposure time and high crowding index and ii) long-distance buses (class II and class III) characterized by long exposure time and a low crowding index. The bus classes are defined by the Regulation n°107 of UNECE on uniform provisions concerning the approval of vehicles, including buses, as shown in Table 1. In class II buses, standing passengers are allowed, although they are unlikely to carry standing people over long distances, making class II and III buses practically identical. Thus, only class III buses were considered in the simulation of long-distance buses.

Infection risk and reproduction numbers are calculated for different scenarios, with ventilation rates estimated according to regulatory standards as well as being measured through an *ad-hoc* experimental campaign, and crowding indexes required by regulatory authorities. For long-distance buses with long exposure times (≥120 min), the room-scale airborne transmission risk will dominate and act to reduce the MRO and consequently increase the effective distances between passengers. For reference, the close proximity risks are negligible beyond 1.75 m in the case of speaking and 0.5 m in the case of breathing (see Supplemental Material). Conversely, for the short exposure time and high crowding of class I buses, the close proximity risk may affect the MRO. As such, the close proximity risk was only specifically considered for urban bus scenarios and, on the basis of the assumption mentioned above, it is negligible for scenarios where commuters wear masks (and thus it has not been considered).

2.3.1. Simulated scenarios

The individual infection risk of susceptible subjects and the reproduction number are evaluated for two types of buses: urban buses (class I) and long-distance buses (class III). The individual bus capacity depends on the size of the vehicle, the seating configuration, and the regulation regarding standees (Table 2). In the present work, we consider a widely-used conventional bus (Victor and Ponnuswamy, 2012), approximately 12 m long and with a maximum passenger capacity depending on the class in which it is used. The bus dimensions considered in this work are 12 m × 2.55 m × 2.3 m (L × W × H) equal to a volume of 70 m^3. For accurate calculation of the actual internal volume, the volume occupied by the seats is removed as well as the volume occupied by passengers. The crowding index, suggested by Regulation n°107 (ECE-R107, 2015) on the uniform provisions concerning the approval of vehicles, including buses, amounts to 93 and 51 occupants (seated + standees, excluding the driver) for class I and class III buses, respectively. Considering a density of humans of 1010 kg m^{-3} (Deziel, 2021), the mass of a passenger of 68 kg (ECE-R107, 2015), and the crowding index expected by Regulation n°107 (ECE-R107, 2015; Table 2), the volume occupied by passengers is 6 m^3 and 3 m^3 for class I and class III, respectively. Moreover, the volume occupied by the seats expected by Regulation n°107 (ECE-R107, 2015) is equal to 1.4 m^3 and 2 m^3, for class I and class III, respectively.

The heating, ventilation and air conditioning (HVAC) system plays a key role in the airborne transmission of respiratory infections within a bus because it adds clean, pathogen-free air to the indoor environment as a fraction of its flow rate. The data on buses and HVAC systems have been found by consulting technical data sheets provided by manufacturers. The considered HVAC system can provide a maximum flow rate of 4400 m^3 h^{-1} including both recirculated air and outdoor fresh air. Detailed legislation on the

Table 1
Classes of buses according to Regulation n°107 of the UNECE (ECE-R107, 2015).

Class I buses	Vehicles constructed with areas for standing passengers, to allow frequent passenger movement
Class II buses	Vehicles constructed principally for the carriage of seated passengers and designed to allow the carriage of standing passengers in the gangway and/or in an area that does not exceed the space provided for two double seats
Class III buses	Vehicles constructed exclusively for the carriage of seated passengers

Table 2
Characteristics of the buses in terms of maximum occupancy, volume, crowding index, and ventilation rate.

Bus class	Maximum occupancy suggested by the (ECE-R107, 2015) regulation			Volume (m^3)	Crowding index (person m^{-3})	Air exchange rate due to outdoor fresh air (EN 1432–1) (h^{-1})
	Seats	Standees	Tot			
I	36	57	93	63	1.5	22
III	51	–	51	65	0.8	12

minimum outdoor fresh air to be supplied in buses is missing, thus the reference value for urban and suburban rolling stock, suggested by EN 1432-1 (2006), is typically adopted: it is equal to 15 m^3 h^{-1}-person^{-1} (i.e. ~4.17 L s^{-1} person^{-1}) or 22 h^{-1} and 12 h^{-1} for class I and III, respectively (Table 2). The recirculated air should be treated using filters able to capture and remove particles with different efficiencies depending on the filter used. If this does not occur, the recirculated air will not enhance the air exchange rate guaranteed by the outdoor air supply. In the simulations performed here, we considered three different efficiencies for filtering the recirculated air: no filtration, filtration through a G3 filter, and filtration through a M6 filter (ISO 16890-1, 2016). All the simulations for urban buses were carried out with no filtration of the recirculated air. Considering the distribution of the particles emitted by an infected subject during speaking (distribution post-evaporation fitted by seven size ranges as reported in Cortellessa et al.(2021), and the efficiency declared by regulation ISO 16890-1 (2016), the filters guarantee a weighted average removal efficiency of 4% for G3 and 40% for M6 filters, respectively.

The actual air exchange rate in buses is also affected by the opening of windows and doors, which increases the air exchange rate. This typically occurs in urban buses, which are characterized by frequent stops, when doors must be opened, and high crowding indexes leading to windows being kept open. For this reason, the actual ventilation rate for urban buses (class I) were measured through an *ad-hoc* experimental campaign as described in Section 2.3.2.

The simulations are performed considering one infected passenger (I = 1) in a fully susceptible population. We point out that the proposed methodology would easily allow simulating further scenarios with more than one infected subject. Nonetheless, for the sake of brevity we limited the simulations to one infected subject; indeed, one infected over 93 passengers represents an extremely high percentage (roughly 1%) which is larger than the typical infection rate occurring worldwide during the pandemic. The exposed susceptibles were considered to be performing activities in sitting and standing positions and inhaling at IR = 0.54 m^3 h^{-1} (Adams, 1993; ICRP, 1994). Travel times on buses vary widely between urban and long-distance buses depending on the number of stops, travel distance, and traffic patterns. The travel time considered is: (i) 24 min for urban buses (class I), which is the average time spent by a commuter on an urban bus in Italy (ISTAT, 2019); and (ii) travel time up to 8 h for long-distance buses (class III). The urban bus scenarios were simulated considering that all the 93 commuters stayed simultaneously for 24 min in the bus. This is a rare case, but it represents the worst situation and should be considered as a conservative approach.

Our modelling scenarios also consider the use of face masks by bus passengers, because universal masking has been a primary public health strategy during the COVID-19 pandemic. In the scenarios with this mitigation solution, all the commuters wear a mask, both infected and susceptible, and we consider both surgical and FFP2 masks. For the surgical masks, we assume a 40% reduction in inhaled particles (Eikenberry et al., 2020), seen as the product of the reduction of the emission of the infected subject and the inhalation of the susceptibles. For the FFP2 masks, the overall considered reduction effect was assumed to be 80% (Poydenot et al., 2021). These values take into account the actual use of the mask, not just the nominal efficiencies of the filter media.

Emission and exposure assumptions for the scenarios in the prospective assessment for urban buses (class I) and long-distance buses (class III) are summarized in Tables 3 and 4, respectively.

Table 3
Scenarios simulated for urban buses (class I): emission duration and respiratory activity. Descriptions of the scenarios and the activity mitigation solutions are reported. All the simulations were carried out with the actual air exchange rates and with no filtration of the recirculated air.

Scenarios		Emission duration (min) and respiratory activity	Description
Base scenario	C-0-UB	24 min, oral breathing	Infected commuter standing for the whole trip oral breathing. No filtration of the recirculated air.
Speaking effect & windows closed	C-24-UB	24 min, speaking	Infected commuter standing for the whole trip speaking and with windows closed. No filtration of the recirculated air.
Speaking effect & windows opened	C-24-UB-WO	24 min, speaking	Infected commuter standing for the whole trip speaking and with windows opened. No filtration of the recirculated air.
Surgical mask, speaking effect & windows closed	C-24-UB-SM	24 min, speaking	Infected commuter standing for the whole trip speaking, all commuters wearing a surgical mask and with windows closed. No filtration of the recirculated air.
FFP2 mask, speaking effect & windows closed	C-24-UB-FFP2	24 min, speaking	Infected commuter standing for the whole trip speaking, all commuters wearing an FFP2 mask and with windows closed. No filtration of the recirculated air.
Surgical mask, windows open & speaking effect	C-24-UB-SM + WO	24 min, speaking	Infected commuter standing for the whole trip speaking, all commuters wearing a surgical mask and with windows opened. No filtration of the recirculated air.
FFP2 mask, windows open & speaking effect	C-24-UB-FFP2 + WO	24 min, speaking	Infected commuter standing for the whole trip speaking, all commuters wearing an FFP2 mask and with windows opened. No filtration of the recirculated air.

Table 4
Scenarios simulated for long-distance buses (class III): emission duration and respiratory activity. Descriptions of the scenarios and the activity mitigation solutions are reported. All the simulations of the long-distance buses were carried out with the air exchange rates suggested by the standard.

Scenarios		Emission duration (min) and respiratory activity	Description
Base scenario	C-0-LDB	480 min oral breathing	Infected commuter standing for the whole trip oral breathing. No filtration of the recirculated air.
Commuter's speaking effect	C-30-LDB	30 min speaking & 450 min oral breathing	Infected commuter speaking for the first 30 min and oral breathing for the rest of the time. No filtration of the recirculated air.
	C-60-LDB	60 min speaking & 420 min oral breathing	Infected commuter speaking for the first 60 min and oral breathing for the rest of the time. No filtration of the recirculated air.
Filtration G3 & speaking effect	C-60-LDB-G3	60 min speaking & 420 min oral breathing	Infected commuter speaking for the first 60 min and oral breathing for the rest of the time. The recirculated air is filtered with a G3 filter.
Surgical mask effect	C-0-LDB-SM	480 min oral breathing	Infected commuter standing for the whole trip oral breathing. All commuters wear surgical masks. No filtration of the recirculated air.
Filtration M6 effect	C-0-LDB-M6	480 min oral breathing	Infected commuter standing for the whole trip oral breathing. The recirculated air is filtered with an M6 filter.
Filtration M6 & speaking effect	C-60-LDB-M6	60 min speaking & 420 min oral breathing	Infected commuter speaking for the first 60 min and oral breathing for the rest of the time. The recirculated air is filtered with an M6 filter.
Surgical mask & speaking effect	C-60-LDB-SM	60 min speaking & 420 min oral breathing	Infected commuter speaking for the first 60 min and oral breathing for the rest of the time. All commuters wear surgical masks. No filtration of the recirculated air.
FFP2 & speaking effect	C-60-LDB-FFP2	60 min speaking & 420 min oral breathing	Infected commuter speaking for the first 60 min and oral breathing for the rest of the time. All commuters wear an FFP2 mask. No filtration of the recirculated air.
FFP2 & filtration M6 effect	C-60-LDB-FFP2 + M6	60 min speaking & 420 min oral breathing	Infected commuter speaking for the first 60 min and oral breathing for the rest of the time. The recirculated air is filtered with an M6 filter and all commuters wear a surgical mask.

2.3.2. Measurement of the air exchange rate for buses class I

The actual air exchange rate for urban buses (class I) was determined through in-field measurements using the decay method of a tracer gas (Van Buggenhout et al., 2009; Cui et al., 2015; ISO 12569, 2017). In brief, a dose of tracer gas is injected and mixed with the air inside the bus. When the injection is stopped, the concentration peak is reached and the tracer gas concentration begins to decrease and is recorded during a given period. The tracer gas decay method is based on the mass balance of the tracer gas which allows the air exchange rate (AER, h^{-1}) to be calculated through the exponential decay equation:

$$AER = \frac{ln\frac{(C_{peak}-C_{out})}{(C_{final}-C_{out})}}{\Delta t}(h^{-1}) \quad (9)$$

where C_{peak}, C_{final}, and C_{out} represent the initial peak, final, and outdoor tracer gas concentrations, respectively, and Δt the time interval between C_{peak} and C_{final}.

In the experimental campaign, carbon dioxide (CO_2) was used as a tracer gas. Measurements were conducted with six Onset HOBO MX1102 CO_2 data loggers (Range 0 to 5000 ppm CO_2, accuracy ± 50 ppm ± 5%) and a Testo 435 multifunctional logger with IAQ (Range 0 to 10000 ppm - Accuracy: 0 to 5000 ppm CO_2, ±75 ppm ± 3%; 5000 to 10000 ppm CO_2, ±150 ppm ± 5%). Before the measurement campaign, the sensors were calibrated by using pure nitrogen and an analytically calibrated gas mixture with a concentration of 4000 ppm CO_2 in nitrogen.

The measurements were carried out in a bus used for urban transport, namely IIA City Mood bus (class I) on an ordinary route and the measurements were carried out both with the windows closed and the windows open. The vehicle was provided for 4 side windows with a sliding opening (1/3 of height) with an overall area of 0.96 m^2 (when fully opened). The experimental runs were carried out on a not windy day, so the air change is mainly due to the bus motion. The ventilation system of the buses was kept in operation for the entire duration of the tests. During the measurements, only the operator and the driver were on the bus. Three different measurements for each driving condition (closed/open window) were conducted. In each run the CO_2 concentration was pushed up to 5000 ppm while the vehicle was in motion, then its decay was recorded not considering stops and traffic lights. The sensors were placed at two heights corresponding to the breathing zones for seated (1.10 m) and standing (1.70 m) passengers. The four sensors measuring at the breathing zone of seated person (1.10 m above the ground) were placed at 25% and 75% of the total length of the vehicle. In the case of two rows of seats, the two sensors were placed between the abreast seating, whereas in the case of single-seat, the sensor was placed on the aisle-side seat. The two sensors measuring at the breathing zone of standing person (1.70 m above the ground) were placed on the centerline of the vehicle between the two doors and between the rear door and the back of the vehicle. We point out that the CO_2 concentration was measured at several points in the bus because the variable vehicle speed and the repeated opening of doors did not allow the tracer gas concentration to achieve uniformity. During a single run, the difference of concentration of CO_2 measured by the different sensors placed in the vehicle exceeds 1000 ppm. The CO_2 concentration values measured at each point were processed according to the decay method to calculate the local value of the air exchange rate and, finally, the average value of AER was calculated. Illustrative examples of CO_2 decay trends for both windows open and closed conditions are reported in Supplementary Data (Figs. S1 and S2). The measurements collected in the experimental campaign are shown in Table 5. All values reported in Table 5 rep-

Table 5
Actual air exchange rates (AER) measured for urban bus IIA CityMood bus (class I) during the experimental analyses. Data are reported as average ± standard deviation values.

Experiment	AER (h^{-1})	Ventilation rate per person (L s^{-1} $person^{-1}$)
Windows open	65.3 ± 4.6	12.4 ± 0.9
Windows closed	26.9 ± 3.9	5.1 ± 0.7

resent the average values of the three runs. For the calculation of the air change rate, only CO_2 concentration values >800 ppm have been considered. The data clearly show that for the windows closed condition, the minimum AER due to outdoor fresh air suggested by the EN 1432-1 standard (22 h^{-1}, i.e. 4.17 L s^{-1} $person^{-1}$) is guaranteed; indeed, the experimental AER value with windows closed is slightly larger than the value suggested by the standard, likely due to the frequent stops of the bus during which the doors were opened. However, when the windows were kept open during the whole trip, the actual AER was roughly three times the prescribed value, reaching 65.3 h^{-1}.

3. Results and discussions

3.1. Urban buses

Fig. 1 presents the close proximity and room-scale individual risks after 24 min for the breathing (C-0-UB) and speaking (C-24-UB) scenarios. The room-scale risk in the case of windows open for enhanced ventilation (C-24-UB-WO) is also shown. For the speaking scenario, the close proximity risk exceeds the room-scale risk for separation distances below approximately 1.5 m; in particular, the close-proximity individual risk is extremely high (~75%) in the case of full occupancy of the bus (93 persons, which means an average separation distance of 0.32 m). Because we assumed that an infected person has close proximity interaction with only one susceptible person, the maximum R_{cp} value (resulting from a separation distance of 0.32 m) is about 0.75. Conversely, for the breathing scenario, the close proximity risk is only higher than the room-scale one when the infected person is within 0.2 m of a susceptible person, and the close proximity risk is very low (~0.2%) at the designed distance of 0.32 m. As such, the close proximity risk for breathing has a minimal impact on the reproduction number for the scenarios evaluated here, and can be omitted from all R_{event} calculations. Indeed, in the case of an infected subject breathing for the entire trip, the IR_{rs} is 0.48%, and the R_{rs} = R_{event} = 0.44 (i.e. calculated as the product between 0.48% and the 92 susceptibles); therefore, the full occupancy suggested by the ECE-R107 (2015) regulation (93 commuters) is satisfied.

In contrast with the breathing scenarios, for an infected subject speaking during the whole trip, the R_{event}, and then the MRO, is also significantly affected by the close proximity risk of infection due to its high IR_{cp}. The effect of close proximity to the total R_{event} becomes even more predominant when the number of susceptibles decreases (i.e. when the R_{rs} decreases). This is clearly shown in Fig. 2, where the R_{cp} was added to the R_{rs} to calculate the total R_{event} value for C-24-UB and C-24-UB-WO scenarios. The graphs show that to maintain R_{event} < 1 on the urban buses when the infected subject is speaking, it is necessary to reduce the MRO to 40 persons and 23 persons for the scenarios with windows open and closed (corresponding to distances of approximately 0.5 m and 0.65 m), respectively. These values are approximately halved with respect to the MRO values considering R_{rs} alone. Therefore, to avoid a reduction of the occupancy, it would be necessary to keep the windows open in urban buses and adopt other strategies such as wearing masks. Indeed, the occupancy imposed by the regulation (93 persons) would guarantee a R_{event} < 1 when FFP2 masks are worn (both with windows closed or open; i.e. scenarios C-24-UB-FFP2 and C-24-UB-FFP2 + WO reported in Supplementary Data Fig. S3) or when surgical masks are worn with the windows kept open (scenario C-24-UB-SM + WO). In contrast, with the windows closed, the MRO would be <93 even if all the commuters were wearing surgical masks (scenario C-24-UB-SM with an MRO = 80). Once again, we highlight that the close proximity risk was assumed to be negligible when the commuters wear a mask; thus, for those scenarios, the R_{event} (and the MRO) is only related to the room-scale risk.

3.2. Long-distance buses

For long-distance buses, the susceptibles travel for a long time (up to 480 min according to the investigated scenarios) in the same confined space with an infected subject, causing the IR_{rs} to increase, and thus increasing the R_{event}. We point out that for long-distance buses, the R_{event} is equal only to the room-scale reproduction number because the distances and the orientation between the commuters are such as to consider R_{cp} negligible. Fig. 3 shows an illustrative example of quanta concentration, IR_{rs} and MRO trends for the scenario characterized by an infected com-

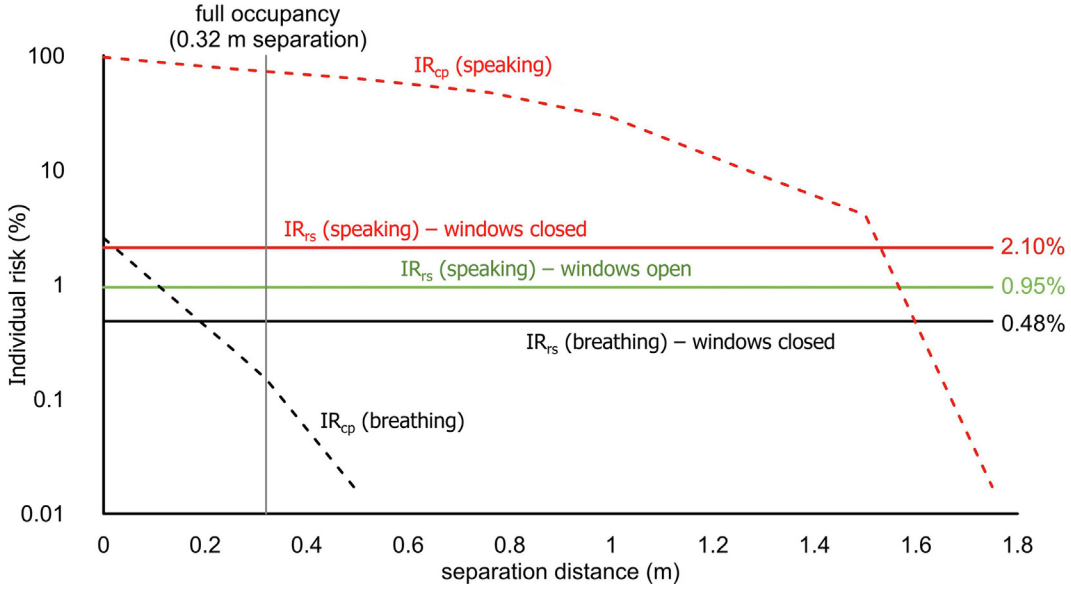

Fig. 1. Close proximity risk (IR_{cp}) as a function of separation distance for the Delta variant for 24 min of breathing and speaking, as compared with room-scale airborne transmission risk (IR_{rs}) for the C-0-UB (breathing, windows closed), C-24-UB (speaking, windows closed), and C-24-UB-WO (speaking, windows open) scenarios.

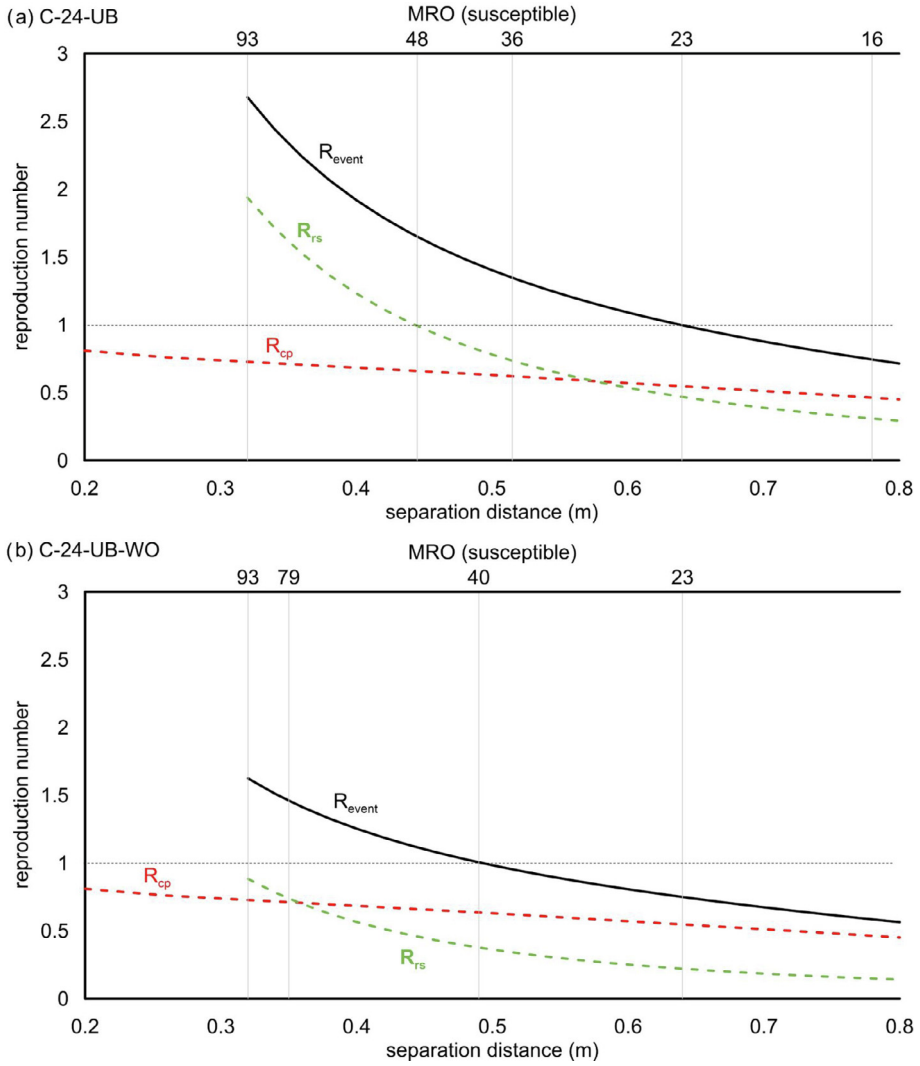

Fig. 2. R_{event} considering both close proximity (R_{cp}) and room-scale (R_{rs}) contributions for the C-24-UB (a) and C-24-UB-WO (b) scenarios. The equivalent maximum room occupancies (MROs) for maximum occupancy (93), $R_{rs} < 1$, and $R_{event} < 1$ are denoted by vertical lines.

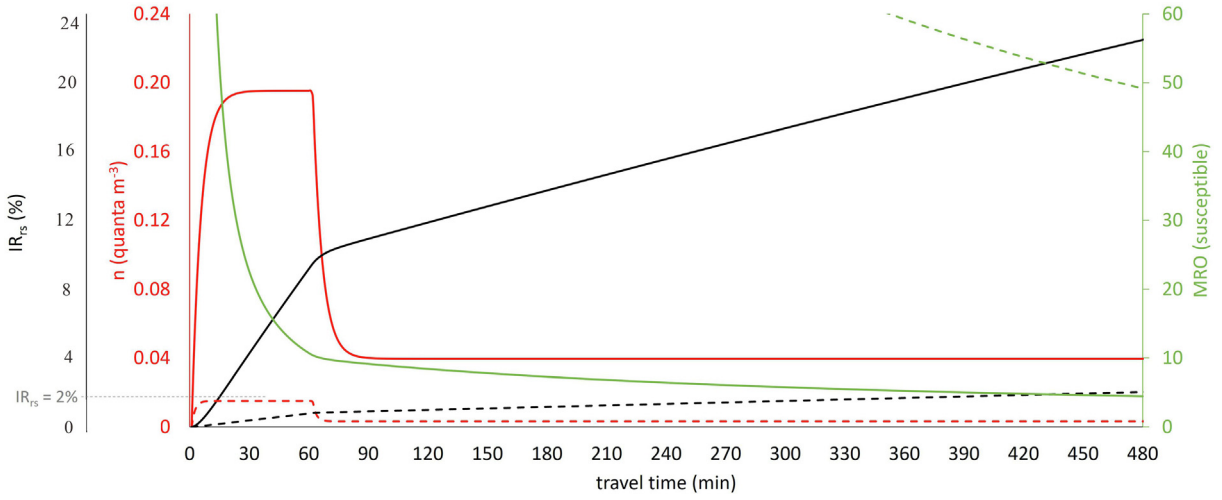

Fig. 3. Trends of quanta concentration (n), individual room-scale risk (IR_{rs}) and maximum room occupancy (MRO) for C-60-LDB (solid lines) and C-60-LDB-FFP2 + M6 (dotted lines) scenarios.

muter speaking for 60 min with no mitigation measures (case C-60-LDB). In this scenario, the IR_{rs} reaches the maximum permitted value in 16 min (2%; i.e. 1 over 50 susceptible exposed persons), staying above that value for the entire travel time and thus not allowing full occupancy of the bus.

Table 6 shows the required MRO to maintain $R_{event} < 1$ for all the investigated scenarios for long-distance buses. For the C-60-LDB scenario, the MRO is extremely low even for a 1 h travel time (only 11 susceptibles could simultaneously share the bus) dropping to 4 commuters for an 8 h trip. The maximum occupancy of the bus is clearly related to the speaking time of the infected person during the trip (as also graphed in Fig. 4). Indeed, when the speaking time is reduced to 30 min (C-30-LDB scenario) or 0 min (C-0-LDB, i.e. infected person only breathing) the MRO slightly increases but it is still far from the full occupancy. Nonetheless, full occupancy of the bus can be adopted for a 1 h travel time in the case of an infected individual only breathing. The use of surgical masks does not significantly improve the occupancy of the bus because, once again, full occupancy would be allowed only for a 1 h travel time as shown in Fig. 4. Therefore, unless frequent breaks were taken during the trip to significantly lower the quanta concentration in the bus, further mitigation measures are needed to safely increase the number of commuters. In fact, the MRO data reported in Table 6 clearly highlight the fact that enhancing the ventilation through appropriate filtration of the recirculated air (M6 filter) and/or the use of more effective masks (FFP2) increases the MRO; indeed, when these two mitigation solutions are adopted simultaneously even for an infected subject speaking for 1 h, full occupancy would be permitted for very long trips. This is clearly illustrated in Fig. 3 which shows the IR_{rs} and MRO trends for the C-60-LDB-FFP2 + M6 scenario: the individual risk IR_{rs} remains below the maximum permitted value (2%) up to 457 min and the MRO for an 8 h travel time is 49 commuters (i.e. almost full occupancy). The scenarios here analyzed considered a continuous exposure of 8 h, actually, according to the European Regulation (European Commission, 2006), after a driving period of four and a half hours the bus driver have to take an uninterrupted break of not <45 min. For the most critical scenario analyzed (and reported in Fig. 3), C-60-LDB, the individual risk after four and a half hours would be equal to roughly 17% then resulting in a maximum occupancy of 6 persons which is quite similar to the MRO at 480 min (4 persons). In the paper we have not considered exposure scenarios of 8 h with a 45 min break after four and a half hours since this would have resulted defining other sub-scenarios for the break period (e.g. during the break is the HVAC system switched off or on? Are the passengers inside or outside the bus? etc.); some of these scenarios would lead to an overall 8 h risk not necessarily less critical with respect to those with no breaks. Summarizing, our choice represents a particular scenario considering the HVAC system switched on and the passenger inside the bus during the break.

When adequate filtration of the recirculated air and FFP2 masks are not adopted, the only solution to increase the MRO in long-

Table 6
Maximum room occupancy for long-distance buses to maintain a $R_{event} < 1$ as a function of the scenarios investigated.

Scenarios		Travel time			
		60 min	120 min	240 min	480 min
Base scenario	C-0-LDB	*	25	13	7
Commuter's speaking effect	C-30-LDB	15	12	8	5
	C-60-LDB	11	8	6	4
Filtration G3 & speaking effect	C-60-LDB-G3	12	10	7	5
Surgical mask effect	C-0-LDB-SM	*	42	21	11
Filtration M6 effect	C-0-LDB-M6	*	*	30	15
Filtration M6 & speaking effect	C-60-LDB-M6	26	21	15	10
Surgical mask & speaking effect	C-60-LDB-SM	18	14	10	7
FFP2 & speaking effect	C-60-LDB-FFP2	51	40	30	20
FFP2 & filtration M6 effect	C-60-LDB-FFP2 + M6	*	*	*	49

*The occupancy suggested by the ECE-R107 (2015) regulation is satisfied.

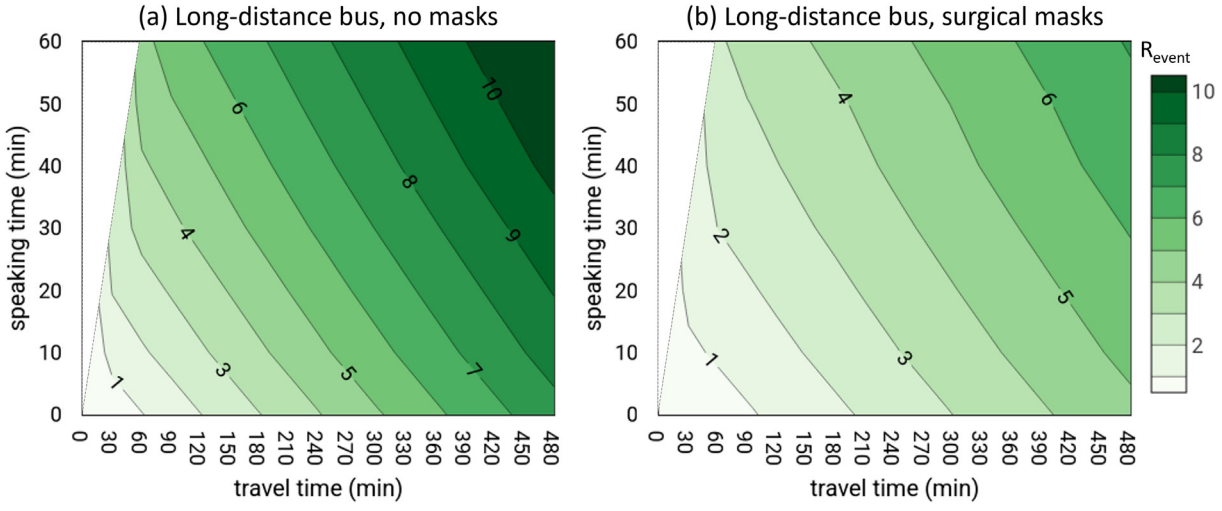

Fig. 4. R_{event} as a function of speaking time (from 0 to 60 min) and travel time (from 0 to 480 min): (a) infected commuter speaking for the first minutes (0 to 60 min) and oral breathing for the rest of the time; (b) infected commuter speaking for the first minutes (0 to 60 min) and oral breathing for the rest of the time, with all commuters wearing surgical masks.

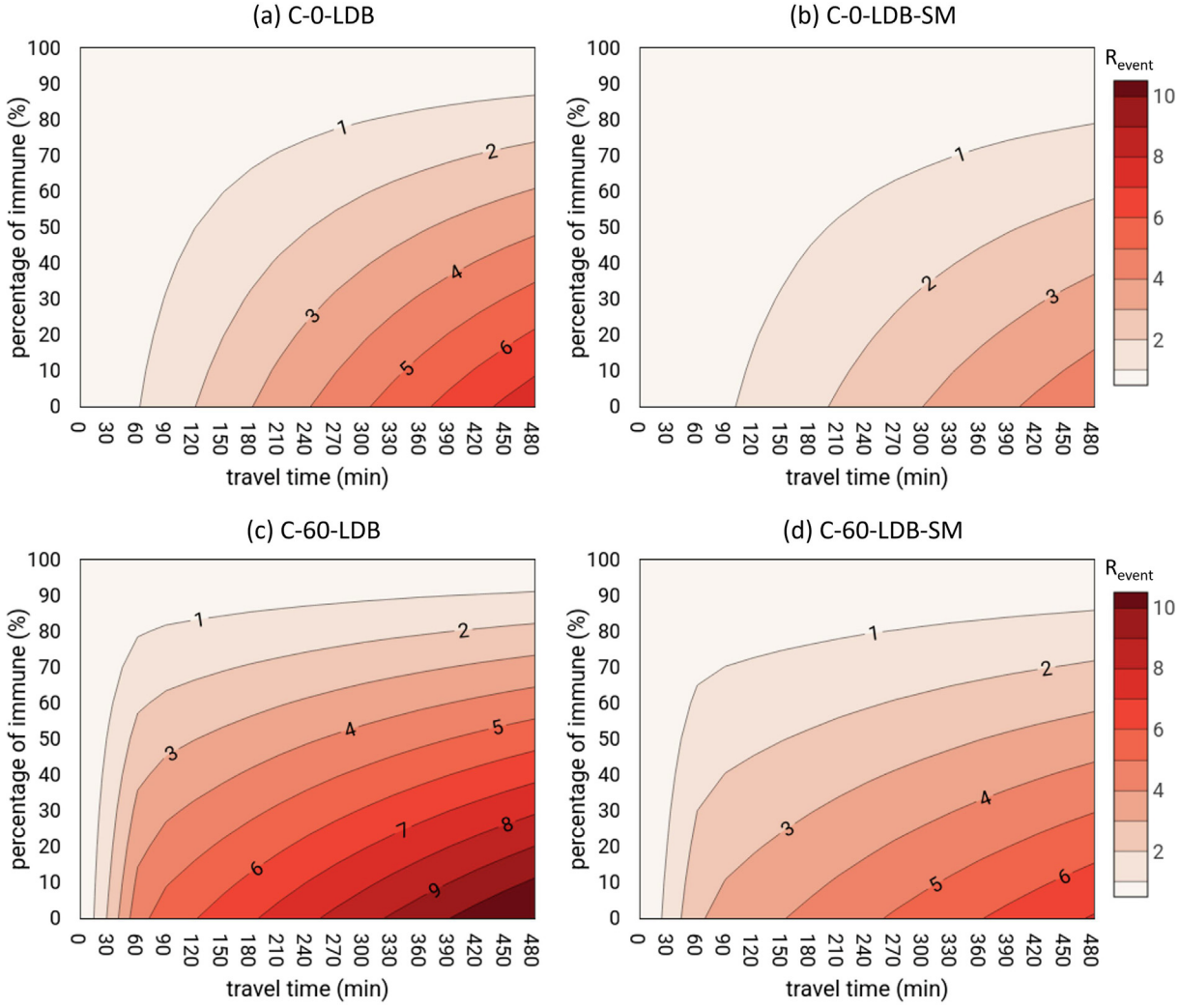

Fig. 5. R_{event} as a function of the percentage of immune individuals and travel time (from 0 to 480 min): (a) C-0-LDB, infected commuter standing for the whole trip oral breathing; (b) C-0-LDB-SM, infected commuter standing for the whole trip oral breathing and all commuters wear surgical masks; (c) C-60-LDB, infected commuter speaking for the first 60 min and oral breathing for the rest of the time and all commuters wear surgical masks; and (d) C-60-LDB-SM, infected commuter standing for the whole trip oral breathing and all commuters wear surgical masks.

distance buses is to reduce the number of susceptible people amongst those exposed; in other words, the fraction of the immune population (e.g. by vaccination) should be increased. To this end, Fig. 5 shows the R_{event} in long-distance buses as a function of the percentage of immunization (simulated by changing artificially the number of susceptibles) and travel time (from 0 to 480 min) in the cases of breathing without mitigation measures (C-0-LDB), breathing with surgical masks (C-0-LDB-SM), speaking without mitigation measures (C-60-LDB), and speaking with surgical masks (C-60-LDB-SM). The figures indicate that, as expected, the presence of the immunes can reduce virus transmission; nonetheless, only a percentage of immunes higher than 90% would allow a $R_{event} < 1$ in the case of 480-min trips with no masks. In fact, even if surgical masks were worn, a high percentage of immunes would still be required, i.e. at least 80% and 85% for oral-breathing and speaking activities, respectively.

4. Conclusions

This study evaluates the individual risk and the potential transmissibility (i.e. reproductive number, R_{event}) of SARS-CoV-2 infection in public buses, both in urban buses (characterized by a shorter exposure time but a higher crowding index) and long-distance buses (longer exposure time, lower crowding index). We considered the risk due to the proximity to the infected subject (close proximity contribution) and the risk related to the accumulation of virus-laden droplets in buses (also not in close proximity, i.e. room-scale contribution). Several typical scenarios in terms of ventilation, travel time, and expiratory activity of the infected subject are evaluated, as well as the adoption of mitigation strategies.

For urban buses, the contribution of close proximity to the individual risk is extremely high when the infected subject speaks for the entire travel time (up to 75% for full occupancy of the bus, i.e. at a separation distance of 0.32 m), thus significantly contributing to the reproductive number and, consequently, to the maximum occupancy of the bus in view of controlling the transmissibility of the pandemic. Indeed, the maximum occupancy to guarantee a $R_{event} < 1$ (MRO) would be lower than the full occupancy of the bus both with the windows closed (measured ventilation rate of about 27 h^{-1}, MRO = 23 commuters) and with windows open (measured ventilation rate of about 65 h^{-1}, MRO = 40 commuters). To maintain a $R_{event} < 1$ for full occupancy of the bus, masks should be adopted (FFP2 with the windows closed). For a breathing infected subject, the close proximity risk is negligible, and the room-scale contribution is 0.48%, thus guaranteeing a $R_{event} < 1$ with full occupancy of the bus.

For long-distance buses, the close proximity contribution can be reasonably neglected due to the distances and orientation amongst the commuters; thus, the risk is only related to the room-scale contribution. The total exposure (travel) time and the adoption of mitigation solutions significantly affect the maximum occupancy of the bus. Reducing the speaking time and adopting frequent breaks during the trip represent very basic solutions that cannot always be applied. As an example, in the case of an infected person speaking for 1 h, only high quality filtration of the recirculated air and the simultaneous use of FFP2 masks would permit full occupancy of the bus up to almost 8 h; otherwise, an extremely high percentage of immunized persons (>80%) would be required.

Declaration of Competing Interest

The authors declare that they have no known competing financial interests or personal relationships that could have appeared to influence the work reported in this paper.

Appendix A. Supplementary data

Supplementary data to this article can be found online at https://doi.org/10.1016/j.gsf.2022.101398.

References

Adams, W.C., 1993. Measurement of Breathing Rate and Volume in Routinely Performed Daily Activities. Final Report.

Arpino, F., Cortellessa, G., Dell'Isola, M., Massarotti, N., Mauro, A., 2014. High order explicit solutions for the transient natural convection of incompressible fluids in tall cavities. Numer. Heat Transf. Part Appl. 66, 839–862. https://doi.org/10.1080/10407782.2014.892389.

ASHRAE 62.1, 2019. Standard 62.1 - Ventilation for Acceptable Indoor Air Quality.

Blocken, B., van Druenen, T., van Hooff, T., Verstappen, P.A., Marchal, T., Marr, L.C., 2020. Can indoor sports centers be allowed to re-open during the COVID-19 pandemic based on a certificate of equivalence? Build. Environ. 180,. https://doi.org/10.1016/j.buildenv.2020.107022 107022.

Buonanno, G., Morawska, L., Stabile, L., 2020a. Quantitative assessment of the risk of airborne transmission of SARS-CoV-2 infection: Prospective and retrospective applications. Environ. Int. 145,. https://doi.org/10.1016/j.envint.2020.106112 106112.

Buonanno, G., Stabile, L., Morawska, L., 2020b. Estimation of airborne viral emission: Quanta emission rate of SARS-CoV-2 for infection risk assessment. Environ. Int. 141,. https://doi.org/10.1016/j.envint.2020.105794 105794.

Chang, S., Pierson, E., Koh, P.W., Gerardin, J., Redbird, B., Grusky, D., Leskovec, J., 2021. Mobility network models of COVID-19 explain inequities and inform reopening. Nature 589, 82–87. https://doi.org/10.1038/s41586-020-2923-3.

Chatoutsidou, S.E., Lazaridis, M., 2019. Assessment of the impact of particulate dry deposition on soiling of indoor cultural heritage objects found in churches and museums/libraries. J. Cult. Herit. 39, 221–228. https://doi.org/10.1016/j.culher.2019.02.017.

Chen, W., Zhang, N., Wei, J., Yen, H.-L., Li, Y., 2020. Short-range airborne route dominates exposure of respiratory infection during close contact. Build. Environ. 176,. https://doi.org/10.1016/j.buildenv.2020.106859 106859.

Correia, G., Rodrigues, L., Gameiro da Silva, M., Gonçalves, T., 2020. Airborne route and bad use of ventilation systems as non-negligible factors in SARS-CoV-2 transmission. Med. Hypotheses 141,. https://doi.org/10.1016/j.mehy.2020.109781 109781.

Cortellessa, G., Stabile, L., Arpino, F., Faleiros, D.E., van den Bos, W., Morawska, L., Buonanno, G., 2021. Close proximity risk assessment for SARS-CoV-2 infection. Sci. Total Environ. 794,. https://doi.org/10.1016/j.scitotenv.2021.148749 148749.

Cui, S., Cohen, M., Stabat, P., Marchio, D., 2015. CO2 tracer gas concentration decay method for measuring air change rate. Build. Environ. 84, 162–169. https://doi.org/10.1016/j.buildenv.2014.11.007.

Deziel, C., 2021. How to calculate the volume of a person. sciencing.com.

ECE-R107, 2015. Regulation N° 107 of the Economic Commission for Europe of the United Nations (UNECE) — Uniform provisions concerning the approval of category M2 or M3 vehicles with regard to their general construction [2015/922].

Eikenberry, S.E., Mancuso, M., Iboi, E., Phan, T., Eikenberry, K., Kuang, Y., Kostelich, E., Gumel, A.B., 2020. To mask or not to mask: Modeling the potential for face mask use by the general public to curtail the COVID-19 pandemic. Infect. Dis. Model. 5, 293–308. https://doi.org/10.1016/j.idm.2020.04.001.

EN 1432-1, 2006. Railway applications - Air conditioning for urban and suburban rolling stock - Part 1: Comfort parameters.

European Commission, 2006. Regulation (EC) No 561/2006 of the European Parliament and of the Council of 15 March 2006 on the harmonisation of certain social legislation relating to road transport and amending Council Regulations (EEC) No 3821/85 and (EC) No 2135/98 and repealing Council Regulation (EEC) No 3820/85.

Gale, P., 2020. Thermodynamic equilibrium dose-response models for MERS-CoV infection reveal a potential protective role of human lung mucus but not for SARS-CoV-2. Microb. Risk Anal. 16,. https://doi.org/10.1016/j.mran.2020.100140 100140.

Gammaitoni, L., Nucci, M.C., 1997. Using a mathematical model to evaluate the efficacy of TB control measures. Emerg. Infect. Dis. 3, 335–342. https://doi.org/10.3201/eid0303.970310.

Helfand, R.F., Kim, D.K., Gary, H.E., Edwards, G.L., Bisson, G.P., Papania, M.J., et al., 1998. Nonclassic measles infections in an immune population exposed to measles during a college bus trip.

ICRP, 1994. Human respiratory tract model for radiological protection. A report of a Task Group of the International Commission on Radiological Protection. International Commission on Radiological Protection.

ISO 12569, 2017. Thermal performance of buildings and materials - Determination of specific airflow rate in buildings - Tracer gas dilution method.

ISO 16890-1, 2016. Air filters for general ventilation - Part 1: Technical specifications, requirements and classification system based upon particulate matter efficiency (ePM) (ISO 16890-1:2016).

ISTAT, 2019. Uso mezzi e spostamenti.

JT/T 888, 2014. People's Republic of China Transportation Standards JT/T 888-2014, Type dividing and class rating for bus transport.

Kriegel, M., Buchholz, U., Gastmeier, P., Bischoff, P., Abdelgawad, I., Hartmann, A., 2020. Predicted infection risk for aerosol transmission of SARS-CoV-2 (preprint). Occup. Environ. Health. https://doi.org/10.1101/2020.10.08.20209106.

Lednicky, J.A., Lauzardo, M., Fan, Z.H., Jutla, A., Tilly, T.B., Gangwar, M., Usmani, M., Shankar, S.N., Mohamed, K., Eiguren-Fernandez, A., Stephenson, C.J., Alam, M.M., Elbadry, M.A., Loeb, J.C., Subramaniam, K., Waltzek, T.B., Cherabuddi, K., Morris, J.G., Wu, C.-Y., 2020. Viable SARS-CoV-2 in the air of a hospital room with COVID-19 patients. Int. J. Infect. Dis. 100, 476–482. https://doi.org/10.1016/j.ijid.2020.09.025.

Li, Y., Leung, G.M., Tang, J.W., Yang, X., Chao, C.Y.H., Lin, J.Z., Lu, J.W., Nielsen, P.V., Niu, J., Qian, H., Sleigh, A.C., Su, H.-J.-J., Sundell, J., Wong, T.W., Yuen, P.L., 2007. Role of ventilation in airborne transmission of infectious agents in the built environment – a multidisciplinary systematic review. Indoor Air 17, 2–18. https://doi.org/10.1111/j.1600-0668.2006.00445.x.

Liu, Y., Ning, Z., Chen, Y., Guo, M., Liu, Y., Gali, N.K., Sun, L., Duan, Y., Cai, J., Westerdahl, D., Liu, X., Xu, K., Ho, K., Kan, H., Fu, Q., Lan, K., 2020. Aerodynamic analysis of SARS-CoV-2 in two Wuhan hospitals. Nature 582, 557–560. https://doi.org/10.1038/s41586-020-2271-3.

Luo, K., Lei, Z., Hai, Z., Xiao, S., Rui, J., Yang, H., Jing, X., Wang, H., Xie, Z., Luo, P., Li, W., Li, Q., Tan, H., Xu, Z., Yang, Y., Hu, S., Chen, T., 2020. Transmission of SARS-CoV-2 in public transportation vehicles: a case study in Hunan Province, China. Open Forum Infect. Dis. 7, ofaa430. https://doi.org/10.1093/ofid/ofaa430.

Marr, L.C., Tang, J.W., 2021. A paradigm shift to align transmission routes with mechanisms. Clin. Infect. Dis. https://doi.org/10.1093/cid/ciab722 ciab722.

Massarotti, N., Arpino, F., Lewis, R.W., Nithiarasu, P., 2006. Explicit and semi-implicit CBS procedures for incompressible viscous flows. Int. J. Numer. Methods Eng. 66, 1618–1640. https://doi.org/10.1002/nme.1700.

Miller, S.L., Nazaroff, W.W., Jimenez, J.L., Boerstra, A., Buonanno, G., Dancer, S.J., Kurnitski, J., Marr, L.C., Morawska, L., Noakes, C., 2021. Transmission of SARS-CoV-2 by inhalation of respiratory aerosol in the Skagit Valley Chorale superspreading event. Indoor Air 31, 314–323. https://doi.org/10.1111/ina.12751.

Mohr, O., Askar, M., Schink, S., Eckmanns, T., Krause, G., Poggensee, G., 2012. Evidence for airborne infectious disease transmission in public ground transport – a literature review. Eurosurveillance 17. https://doi.org/10.2807/ese.17.35.20255-en.

Morawska, L., Allen, J., Bahnfleth, W., Bluyssen, P.M., Boerstra, A., Buonanno, G., Cao, J., Dancer, S.J., Floto, A., Franchimon, F., Greenhalgh, T., Haworth, C., Hogeling, J., Isaxon, C., Jimenez, J.L., Kurnitski, J., Li, Y., Loomans, M., Marks, G., Marr, L.C., Mazzarella, L., Melikov, A.K., Miller, S., Milton, D.K., Nazaroff, W., Nielsen, P.V., Noakes, C., Peccia, J., Prather, K., Querol, X., Sekhar, C., Seppänen, O., Tanabe, S., Tang, J.W., Tellier, R., Tham, K.W., Wargocki, P., Wierzbicka, A., Yao, M., 2021. A paradigm shift to combat indoor respiratory infection. Science 372, 689–691. https://doi.org/10.1126/science.abg2025.

Morawska, L., Milton, D.K., 2020. It is time to address airborne transmission of coronavirus disease 2019 (COVID-19). Clin. Infect. Dis. https://doi.org/10.1093/cid/ciaa939 ciaa939.

Moreno, T., Pintó, R.M., Bosch, A., Moreno, N., Alastuey, A., Minguillón, M.C., Anfruns-Estrada, E., Guix, S., Fuentes, C., Buonanno, G., Stabile, L., Morawska, L., Querol, X., 2021. Tracing surface and airborne SARS-CoV-2 RNA inside public buses and subway trains. Environ. Int. 147,. https://doi.org/10.1016/j.envint.2020.106326 106326.

Myatt, T.A., Minegishi, T., Allen, J.G., MacIntosh, D.L., 2008. Control of asthma triggers in indoor air with air cleaners: a modeling analysis. Environ. Health 7, 43. https://doi.org/10.1186/1476-069X-7-43.

Nissen, K., Krambrich, J., Akaberi, D., Hoffman, T., Ling, J., Lundkvist, Å., Svensson, L., Salaneck, E., 2020. Long-distance airborne dispersal of SARS-CoV-2 in COVID-19 wards. Sci. Rep. 10, 19589. https://doi.org/10.1038/s41598-020-76442-2.

Perkins, J.E., Bahlke, A.M., Silverman, H.F., 1947. Effect of Ultra-violet Irradiation of Classrooms on Spread of Measles in Large Rural Central Schools Preliminary Report.

Poydenot, F., Abdourahamane, I., Caplain, E., Der, S., Haiech, J., Jallon, A., Khoutami, I., Loucif, A., Marinov, E., Andreotti, B., 2021. Risk assessment for long and short range airborne transmission of SARS-CoV-2, indoors and outdoors, using carbon dioxide measurements. medRxiv 2021.05.04.21256352. https://doi.org/10.1101/2021.05.04.21256352.

Rudnick, S.N., Milton, D.K., 2003. Risk of indoor airborne infection transmission estimated from carbon dioxide concentration: Indoor airborne transmission of infectious diseases. Indoor Air 13, 237–245. https://doi.org/10.1034/j.1600-0668.2003.00189.x.

Scungio, M., Arpino, F., Stabile, L., Buonanno, G., 2013. Numerical simulation of ultrafine particle dispersion in urban street canyons with the Spalart-allmaras Turbulence model. Aerosol Air Qual. Res. 13, 1423–1437. https://doi.org/10.4209/aaqr.2012.11.0306.

Shen, Y., Li, C., Dong, H., Wang, Z., Martinez, L., Sun, Z., Handel, A., Chen, Z., Chen, E., Ebell, M.H., Wang, F., Yi, B., Wang, H., Wang, X., Wang, A., Chen, B., Qi, Y., Liang, L., Li, Y., Ling, F., Chen, J., Xu, G., 2020. Community outbreak investigation of SARS-CoV-2 transmission among bus riders in Eastern China. JAMA Intern. Med. 180, 1665. https://doi.org/10.1001/jamainternmed.2020.5225.

Stabile, L., Pacitto, A., Mikszewski, A., Morawska, L., Buonanno, G., 2021. Ventilation procedures to minimize the airborne transmission of viruses in classrooms. Build. Environ. 202,. https://doi.org/10.1016/j.buildenv.2021.108042 108042.

Stern, R.A., Koutrakis, P., Martins, M.A.G., Lemos, B., Dowd, S.E., Sunderland, E.M., Garshick, E., 2021. Characterization of hospital airborne SARS-CoV-2. Respir. Res. 22, 73. https://doi.org/10.1186/s12931-021-01637-8.

Suleimanov, G.D., Mandokhel, K.K., 1972. Smallpox transmission on a bus / by G.D. Suleimanov Khamal Khan Mandokhel.

Sze To, G.N., Chao, C.Y.H., 2010. Review and comparison between the Wells-Riley and dose-response approaches to risk assessment of infectious respiratory diseases. Indoor Air 20, 2–16. https://doi.org/10.1111/j.1600-0668.2009.00621.x.

Van Buggenhout, S., Van Brecht, A., Eren Özcan, S., Vranken, E., Van Malcot, W., Berckmans, D., 2009. Influence of sampling positions on accuracy of tracer gas measurements in ventilated spaces. Biosyst. Eng. 104, 216–223. https://doi.org/10.1016/j.biosystemseng.2009.04.018.

van Doremalen, N., Bushmaker, T., Morris, D.H., Holbrook, M.G., Gamble, A., Williamson, B.N., Tamin, A., Harcourt, J.L., Thornburg, N.J., Gerber, S.I., Lloyd-Smith, J.O., de Wit, E., Munster, V.J., 2020. Aerosol and surface stability of SARS-CoV-2 as compared with SARS-CoV-1. N. Engl. J. Med. 382, 1564–1567. https://doi.org/10.1056/NEJMc2004973.

VDV 236, 2015. Klimatisierung Von Linienbussen Der Zulassungsklassen 1 UND 2. Fuer Konventionell Angetriebene Diesel- Und Gasbusse Sowie Fuer Hybrid-, Brennstoffzellen- Und Elektrobusse.

Victor, D.J., Ponnuswamy, S., 2012. Urban transportation: planning, operation and management. Tata McGraw-Hill Education.

von Wintersdorff, C., Dingemans, J., van Alphen, L., Wolffs, P., van der Veer, B., Hoebe, C., Savelkoul, P., 2021. Infections caused by the Delta variant (B.1.617.2) of SARS-CoV-2 are associated with increased viral loads compared to infections with the Alpha variant (B.1.1.7) or non-Variants of Concern. Res. Sq. pre-print.

Wagner, B.G., Coburn, B.J., Blower, S., 2009. Calculating the potential for within-flight transmission of influenza A (H1N1). BMC Med. 7, 81. https://doi.org/10.1186/1741-7015-7-81.

Yang, W., Marr, L.C., 2011. Dynamics of airborne influenza A viruses indoors and dependence on humidity. PLoS ONE 6,. https://doi.org/10.1371/journal.pone.0021481 e21481.